J. Nano- Electron. Phys.
3 (2011) No1, P. 651-661

PACS numbers: 81.15.Gh, 87.15.Pc, 61.05.cp, 03.75.Hh

INTER-ELECTRODE SEPARATION INDUCED AMORPHOUS-TO-NANOCRYSTALLINE TRANSITION OF HYDROGENATED SILICON PREPARED BY CAPACITIVELY COUPLED RF PE-CVD TECHNIQUE

***A.M. Funde*[1], *V.S. Waman*[1], *M.M. Kamble*[1], *M.R. Pramod*[1], *V.G. Sathe*[2], *S.W. Gosavi*[3], *S.R. Jadkar*[3]**

[1] School of Energy Studies,
University of Pune, Pune 411 007, India

[2] UGC-DAE-CSR, University Campus, Khandawa Road,
Indore 452 017, India

[3] Department of Physics,
University of Pune, Pune 411 007, India
Email: sandesh@physics.unipune.ac.in

Role of inter-electrode spacing in capacitively coupled radio frequency plasma enhanced chemical vapor deposition deposition (PE-CVD) system was studied. The influence of inter-electrode separation on the structural, optical and electrical properties of the deposited films was carefully invesigated keeping all other deposition parameters constant. The results indicate that the film growth rate critically depends up on the plasma chemistry/gas phase chemistry altered by variation of inter-electrode separation. Structure and optical properties are strongly influenced by inter-electrode separation. The nanocrystallization in the material was observed for smaller inter-electrode separation, whereas higher inter-electrode separation favors amorphous structure of the deposited material. The band gap of the material was found to decrease from ~2 eV to 1.8 *eV when inter-electrode separation was varied from* 15 *mm to* 40 *mm.*

Keywords: *INTER-ELECTRODE SEPARATION, PE-CVD, HYDROGENATED NANO-CRYSTALLINE SILICON, AMORPHOUS-TO-NANOCRYSTALLINE TRANSITION, FTIR SPECTROSCOPY, RAMAN SPECTROSCOPY.*

(Received 04 February 2011, in final form 13 October 2011)

1. INTRODUCTION

During last three decades or more, hydrogenated amorphous silicon (a-Si:H) has been studied extensively as a basic material for thin film solar cells due to natural abundance of source material, environmental safety, potential high performance and capability of low cost production. Much of progress also have been reported for device application and conversion efficiencies of 11.2 % and 10.2 % have been reported for small area cells and large area panels, respectively [1, 2]. However, the solar cells based on a-Si:H has always been associated with efficiency losses due to light-induced degradation over time [3].

Nowadays, a-Si:H has been replaced by hydrogenated nanocrystalline silicon (nc-Si:H) due to its interesting properties such as high conductivity, high charge carrier mobility and high doping efficiency [4]. Furthermore, nc-Si:H has better stability against light-induced degradation as compared to

a-Si:H counterpart [5]. The radio frequency (RF) plasma enhanced chemical vapor deposition (PE-CVD) is widely preferred method for the deposition of nc-Si:H material. Also, the PE-CVD has been proven for industrial applicability among several direct and indirect methods of deposition of nc-Si:H material.

Material quality in PE-CVD is governed by several deposition parameters. The parameters affecting the deposition conditions and hence material quality of nc-Si:H in PE-CVD are broadly divided in two categories [6], i) Hardware parameters and ii) Process parameters. Both the sets of parameters have been extensively studied for their effect on the material properties. The hardware parameters influencing the material quality are: electrode geometry [7], inter-electrode distance [8], and operating frequency [9]. The process parameters which are easily adjustable for a given reactor are: power density, pressure, substrate temperature, and input gas flows [10]. Much of the research effort is directed towards the understanding of how these externally adjustable parameters affect the internal physical plasma characteristics upon which the material quality of nc-Si:H ultimately depends. The variation of these parameters can significantly alter the plasma properties by affecting the charged particle kinetics, the gas phase chemistry, and the plasma-surface interaction. Setting up the deposition parameters that guarantee a device quality films of nc-Si:H material requires the fundamental understanding of the surface radical reaction mechanism during the film growth. The research targeting better understanding of the reaction mechanisms between the gas-phase species and the deposition surface is of technological importance with potential for improvement in existing technologies. The understanding of deposition mechanism can be achieved by careful study of deposition parameters. This also gives guidelines for determination of optimum deposition conditions for best properties of deposited material. This is achieved by the synergetic effect of different combinations of these plasma parameters resulting in a best quality material.

In literature, there are vivid reports about effect of inter-electrode gap on the properties of material synthesized in capacitively coupled PE-CVD. The control of the electrode gap is important to exploit the high-pressure plasma [11]. The suppression of higher silane-related radicals is probably responsible for preserving good quality at high growth rates because of lower electron temperature in the high pressure and shorter residence time due to the small plasma space. The results obtained by Isomura et al. [11] have demonstrated that the very high growth rate up to ~7 Å/s of a-Si:H films is possible with careful control of the inter-electrode separation. They have shown in the same results that the optical and electrical properties were not deteriorated even at such a high growth rate by PE-CVD at substrate temperature 200 °C. It was also reported that device grade a-Si:H can be produced at practical growth rates without serious thermal damages due to lower substrate temperature to solar cell structures. On the other hand, it also has been observed by Kounavis et al. that at lower inter-electrode separation, the a-Si:H film growth rate was below 1 Å /s [12]. They have also studied the effect of inter-electrode separation on the electronic properties, and found that the reduction in the inter-electrode separation increases defect density. Though the results quoted earlier does not agree on a single conclusion, important conclusion is that there is significant variation in

material properties due to variation in inter-electrode separation. So in order to synthesize nc-Si:H with single governing parameter of inter-electrode separation present study was carried out in silane + hydrogen plasma.

2. EXPERIMENTAL DETAILS

The films were deposited simultaneously on corning glass # 7059 to study optical, electrical and structural properties and c-Si wafers (5-10 Ω·cm, p-type) FTIR study. The corning glass was cleaned in Piranha solution (H_2SO_4:H_2O_2 in the proportion of 4:1) after ultrasonic bath for 5 minutes in distilled water and followed by wash in distilled water. Then dry nitrogen was flush to wipe off water on the glass. The c-Si substrates were treated with HF for two minutes to etch out native oxide layer. The above cleaning method provides good adhesion of the films to substrates. The reaction chamber consists of two capacitive electrodes, out of which, the upper one is grounded and act as substrate holder, which has inbuilt heater to elevate the substrate temperature to desired value.

Table 1 *– Deposition parameters employed to study role of inter-electrode separation*

Sr. No.	Parameter	Value
1	Substrate temperature (T_{sub})	250 °C
2	Inter-electrode separation ($d_{e\text{-}s}$)	15-40 mm
3	Silane flow rate (F_{SiH4})	0.5 sccm
4	Hydrogen flow rate (F_{H2})	75 sccm
5	Deposition pressure (P)	300 mTorr
6	Time of deposition (t)	40 min

The lower electrode, to which RF power is coupled, also acts as gas inlet to reaction chamber. This lower electrode can be moved up/down to adjust the inter-electrode separation. The substrates were loaded on substrate holder and then deposition chamber was evacuated to a base pressure less than 1×10^{-6} Torr. The substrate was heated and brought to 200 °C by appropriately setting the value on controller. After this the reaction gases silane (SiH_4, MSG) and hydrogen (H_2, 99.999 % pure) were introduced from gas inlet through mass-flow controllers. Desired pressure in process chamber was adjusted using throttle valve at suction port of the process chamber. The other deposition parameters are listed in Table 1.

3. RESULTS AND DISCUSSION

3.1 Variation in deposition rate

Figure 3 shows deposition rate (r_d) as a function of inter-electrode separation ($d_{e\text{-}s}$) for nc-Si:H films deposited by PE-CVD method. As seen from figure, with increase in inter-electrode separation up to 30 mm, deposition rate increases however with further increase in inter-electrode separation the deposition rate starts declining. The deposition process in PE-CVD is directly affected by the gas phase reactions occurring in the plasma. A large number of possible gas phase reaction yields in different species in the plasma with varying lifetime. This is a key parameter deciding the

species that reach the film growth surface (substrate) and hence the properties of the deposited material. The steady state density of reactive species in the plasma have been studied with various gas-phase diagnosis techniques and it has been observed that the number density of SiH_3 and H species is more followed by SiH_2, SiH, Si and other low lifetime species [13]. It has been reported that for a fixed deposition pressure, as we go away from the plasma coupling electrode to the substrate holder electrode, the density of SiH_3, the species responsible for growth goes on increases drastically in the initial stage and then saturates [14]. At the same time, by increasing the inter-electrode separation, there is decrease in the density of SiH_3 species in plasma.

This also can be explained on the basis that at lower inter-electrode separation, the residence time of species in the plasma is less and hence the probability of reaching to substrate surface is more for the species responsible for Si:H material growth. This also has limiting value for the present parameters at the inter-electrode separation of 30 mm. When the inter-electrode separation is increased above 30 mm the growth rate starts decreasing. At this increased inter-electrode separation, the residence time of the species in the plasma increases and thereby enhances the probability of secondary gas phase reactions in the plasma. This change in the residence results in the change in the composition of the flux incident onto the growth surface. This results in the declination in the deposition rate for further increase in the inter-electrode separation. The decrease in the deposition rate of a-Si:H with increase in inter-electrode separation was observed previously by Kushaner [14] and Amanatides et al. [15].

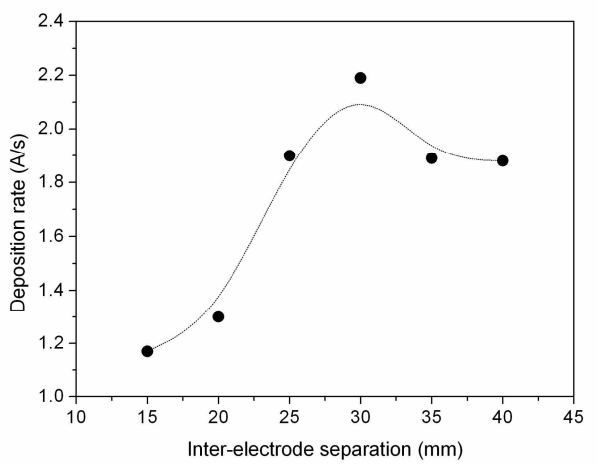

Fig. 1 *– Deposition rate as a function of inter-electrode separation for nc-Si:H films deposited by PE-CVD method. The line drawn is only a guide for eye*

3.2 Raman spectroscopy and low-angle X-ray diffraction analysis

Raman spectroscopy is recognized as a powerful technique for the characterization of Si structures, particularly, for studying nc-Si:H because it gives direct structural evidence quantitatively related to nanocrystalline and amorphous component in it. Figure 2 shows Raman spectra of the films

deposited at various inter-electrode separation ($d_{e\text{-}s}$) in the range 300-600 cm^{-1}. For comparison, Raman spectrum for c-Si is also included in the figure. Raman spectra for samples with $d_{e\text{-}s}$ 15 mm and 20 mm were deconvoluted in the range 400-540 cm^{-1} into two Gaussian peaks and one Lorentzian peak with a quadratic base line method Levenberg-Marquardt method proposed by D.W. Marquardt [16]. Following observations have been made from the Raman spectra for the films deposited at various inter-electrode separations.

I. Films deposited at $d_{e\text{-}s}$ = 15 mm and 20 mm show three transverse optic (TO) phonon modes. These are at ~ 520 cm^{-1} associated with crystalline phase, at ~ 480 cm^{-1} of amorphous phase and the third is in between 500-510 cm^{-1} attributed to small Si crystallites and grain boundaries [17]. For these films crystallite size (d_{Raman}) and volume fraction of crystallites (X_{Raman}) are 8 nm, 6 nm and 56 at.%, 42 at.% respectively. These results indicate that films deposited at lower $d_{e\text{-}s}$ are mixture of two phases, an amorphous phase and a crystalline phase with nano-size Si crystals embedded in amorphous matrix. For films deposited at $d_{e\text{-}s} > 20\ mm$, Raman spectra shows only a broad shoulder centered ~ 480 cm^{-1} associated with a-Si:H.

II. Thus from the Raman spectroscopic analysis it is clear that films deposited with increasing inter-electrode separation an nanocrystalline-to-amorphous transition occurs.

The low angle XRD patterns for the films deposited at various inter-electrode separations were recorded at incidence angle of 1° and are shown in Figure 3. The results are complimentary to the Raman spectroscopic results discussed above. Similar kind of nanocrystalline-to-amorphous transition is also observable in XRD results at $d_{e\text{-}s}$ = 25 mm. Films deposited at $d_{e\text{-}s}$ < 25 mm shows a strong peak at $2\theta \sim 28.14°$ and less intense peaks occur at $2\theta \sim 47.14°$ and ~ 55.75° corresponding to ⟨111⟩, ⟨220⟩ and ⟨311⟩ crystal orientations. The dominant peak is ⟨111⟩. This result indicates that the crystallites in the films have preferential orientation in the ⟨111⟩ directions.

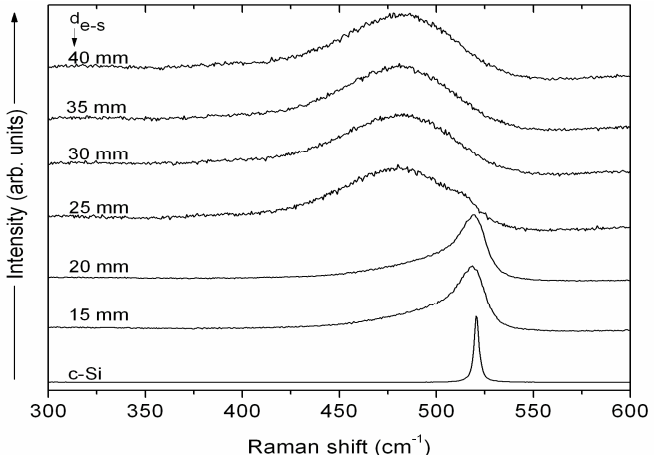

***Fig. 2** – Raman spectra of films deposited at different inter-electrode separation by PE-CVD method*

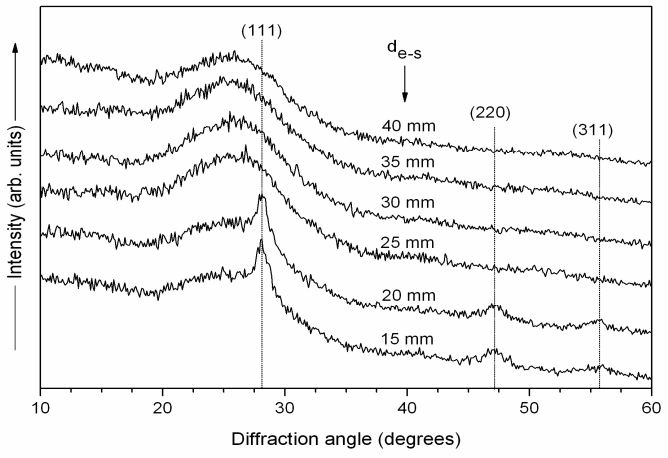

Fig. 3 *– X-ray diffraction patterns of the films deposited at various inter-electrode separations*

The nano-crystallization at $d_{e\text{-}s} < 25$ mm for a fixed other deposition parameters is governed by the gas phase reactions of various species occurring in the plasma before reaching the film growing surface. The three main species of the plasma impinging the film growth surface responsible for properties of the material are SiH_3, H and electrons. Impingement of SiH_3 species on the substrate is believed to be the main species responsible for deposition of nano-crystalline material on substrate in any case. Also, SiH_3 is the only species along with H species having highest density in steady state plasma. At lower $d_{e\text{-}s}$, the probability of SiH_3 species to undergo secondary gas phase reactions and to form other species is less. This results in formation of nanocrystalline material on the substrate surface from the impinging SiH_3 species. The nano-crystallization of the material deposited at lower $d_{e\text{-}s}$ was also observed recently by Chowdhury et al. [18]. They have observed that by increasing the $d_{e\text{-}s}$, the films deposited tend to become amorphous or reduced crystalline fraction depending on the deposition parameters. It also has been reported that at lower $d_{e\text{-}s}$, the electron temperature in the discharge is higher [17] which probably may responsible for the nanocrystalline growth of the film.

The amorphous nature of the films for $d_{e\text{-}s} > 25$ mm may be due to the increased secondary gas phase reactions of SiH_3 species and thus reduced supply of the same on the film growing surface. This results in the depletion in the supply of SiH_3 species and increase in the supply of vibrationally excited silane species to the film growth surface. The impingement of vibrationally excited silane on the film growth surface results in the formation of dust and a-Si:H material. Also, the increase in $d_{e\text{-}s}$, results in the reduced electron temperature in the discharge, whereby electron impact on the film growth surface does not transfer sufficient energy to induce crystallization.

3.3 FTIR spectroscopic analysis

Fourier transform infrared spectroscopy (FTIR) is employed to gain information about the hydrogen bonding structure and hydrogen content in the films. The representative FTIR spectra of films deposited by PE-CVD at various inter-electrode separations ($d_{e\text{-}s}$) are shown in Figure 4. For clarity, spectra have been split horizontally and shifted vertically. It can be seen from FTIR spectra that the films deposited at $d_{e\text{-}s}$ = 15 mm has strong absorption bands ~ 636 cm^{-1} and ~ 2099 cm^{-1}, which correspond to the stretching vibrational modes of mono-hydride, Si-H and di-hydride, $Si\text{-}H_2$ and poly-hydride, $(Si\text{-}H_2)_n$ species [19] respectively. The absorption band ~ 874 cm^{-1} has been also observed and assigned to stretching/bending vibrational modes of di-hydride, $Si\text{-}H_2$ and poly-hydride $(Si\text{-}H_2)_n$ complexes (isolated or coupled) [20] having relatively lesser intensity. Thus, for the films deposited at $d_{e\text{-}s}$ = 15 mm, the hydrogen incorporated in the film is mainly in $Si\text{-}H_2$ and $(Si\text{-}H_2)_n$ bonded species. In addition to these vibrational bands, a strong absorption peak ~ 1014 cm^{-1} associated with the asymmetric Si-O stretching vibration [21] is also observed for the films deposited at $d_{e\text{-}s}$ = 15 mm. This is indicative of an oxidation effect caused by its porous-like microstructure, which is a typical feature for nc-Si:H [22].

Another key observation from the FTIR spectra is the shift of ~ 2090 cm^{-1} absorption band towards 2000 cm^{-1} with increase in inter-electrode separation. Thus, the film deposited at $d_{e\text{-}s}$ = 25 mm and 35 mm the absorption of band ~ 2090 cm^{-1} completely disappear and an absorption ~ 2008 cm^{-1} emerge in the spectrum and its intensity increases with increase in inter-electrode separation. According to the literature the absorption band ~ 2009 cm^{-1} corresponds to the wagging/stretching vibrational modes of mono-hydride, Si-H bonded species [23]. These results indicates that with increase in inter-electrode separation the hydrogen bonding in the films shift from $Si\text{-}H_2$ and $(Si\text{-}H_2)_n$ bonded complexes to Si-H species. This change in hydrogen bonding can be attributed to nanocrystalline-to-amorphous transition with increase in inter-electrode separation as revealed from Raman spectroscopy as well as low angle XRD analysis. It is reported that the hydrogen content (C_H) calculated by different methods is quite different. However, it has been reported that the integrated intensity of the peak ~ 630 cm^{-1} is the best measuring method of hydrogen content and other absorption bands are less reliable [24]. The variation of hydrogen content as a function of inter-electrode separation is shown in Figure 5. As seen from the figure the hydrogen content remains below 12 at. % for the films deposited at $d_{e\text{-}s}$ = 15 mm and 20 mm, but jumps to little more than 17 at. % for the film deposited at $d_{e\text{-}s}$ = 25 mm and then decreases gradually to 15 at. % till $d_{e\text{-}s}$ = 40 mm.

These results clearly indicate that the nanocrystaline films have less bonded hydrogen content than the amorphous counterparts and can attributed to shifting of hydrogen bonding configuration from $Si\text{-}H_2$ and $(Si\text{-}H_2)_n$ bonded complexes to Si-H species with increase in inter-electrode separation.

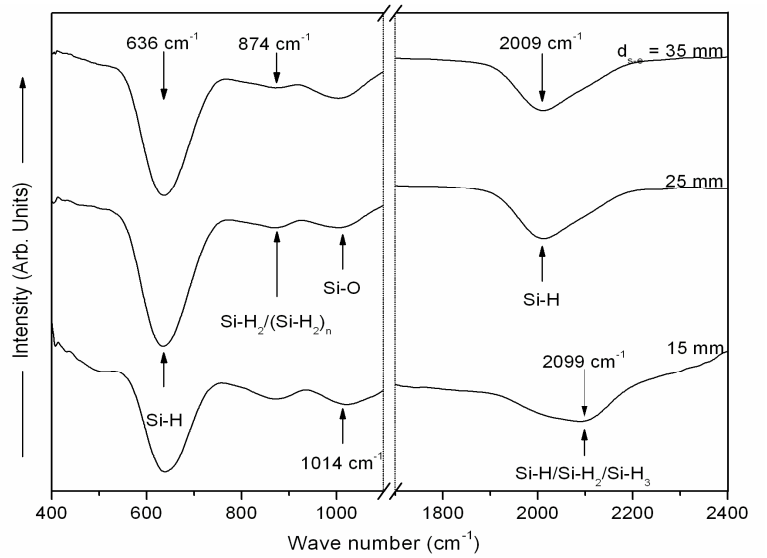

Fig. 4 *– FTIR spectra of some films deposited by PE-CVD at various inter-electrodes separations. Horizontal break between* 1100 cm^{-1} *to* 1700 cm^{-1} *is added for better clarity*

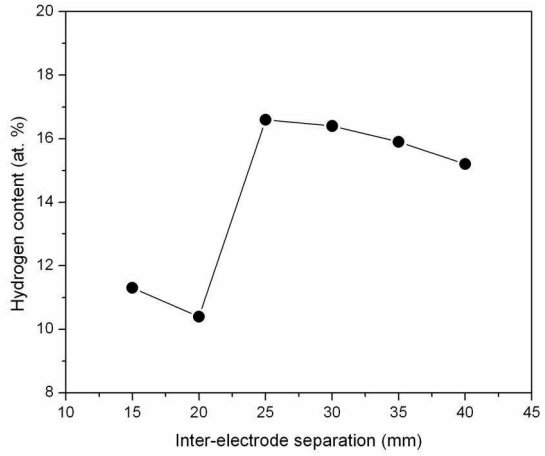

Fig. 5 *– Variation of bonded hydrogen content as a function of inter-electrode separation. The line drawn is guide for eyes*

3.4 Variation in band gap

The band gap (E_g) of the PE-CVD grown films at various inter-electrode separations were investigated from UV-Visible-NIR spectroscopy using Tauc's method. The Figure 6 shows the variation of band gap as a function of inter-electrode separations. As seen from the figure, the films deposited at $d_{e\text{-}s}$ = 15 mm and 20 mm have band gap ~ 2.0 eV which is typical for nc-Si:H films.

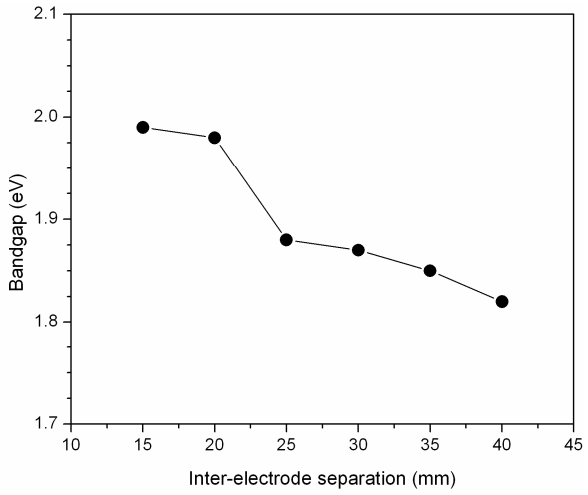

Fig. 6 *– Variation of band gap of the films deposited at different inter-electrode separations*

Indeed, the band gap decreases with increase in inter-electrode separation. The band gap of Si:H is mainly determined by the hydrogen content in the films [25]. The decrease in band gap with increase in inter-electrode separation can be attributed to the decrease in hydrogen content in the films with increase in inter-electrode separation (see Fig. 5).

3.5 Dark conductivity, photo conductivity and photosensitivity

The effect of inter-electrode separation ($d_{s\text{-}e}$) on dark conductivity (σ_{Dark}) and photoconductivity (σ_{Photo}) of Si:H films deposited by PE-CVD is shown in Figure 7. As seen in the figure, the dark conductivity of the films decreases from 1.4×10^{-4} S/cm to 4.7×10^{-10} when inter-electrode separation inc-

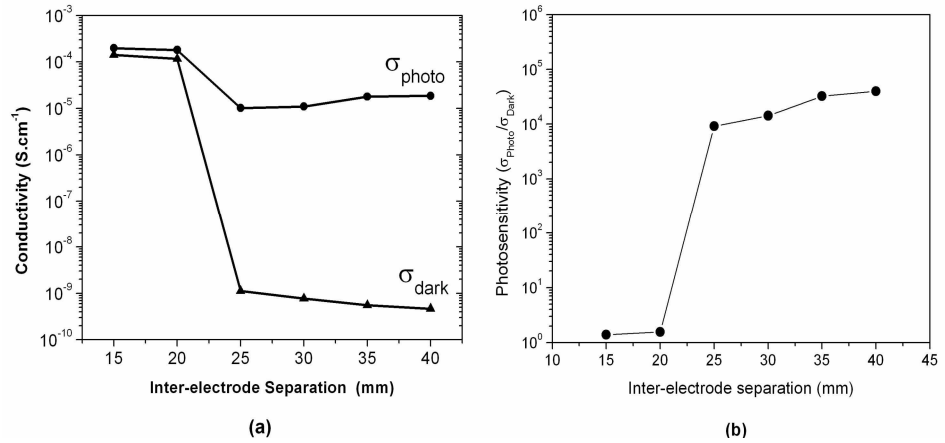

Fig. 7 *– The variation of (a) dark conductivity (σ_{Dark}) as well as photo-conductivity (σ_{Photo}) and (b) photosensitivity ($\sigma_{Dark}/\sigma_{Photo}$) for the films deposited at various inter-electrode separations ($d_{e\text{-}s}$). Lies drawn are guides for eyes.*

reases from 15 mm to 40 mm. This indicates that the films deposited with increasing inter-electrode separation get structurally modified. Furthermore, the photoconductivity of the films remains almost constant in the range 10^{-4}-10^{-5} S/cm over the entire range of inter-electrode separation studied. As a result, the photosensitivity gain, taken as ratio of photoconductivity to dark conductivity ($\sigma_{Photo}/\sigma_{Dark}$) for these films increases from 1.3 to 4×10^5 when inter-electrode separation increased from 15 mm to 40 mm. We attribute the drastic increase in the photosensitivity due the nanocrystalline-to-amorphous transition because the $\mu c/nc$-Si:H films prepared by different methods show high dark conductivity and negligible photosensitivity depending upon the crystallite size and its volume fraction [26]. This inference is further strengthened from Raman spectroscopic and low angle XRD results.

4. CONCLUSIONS

An attempt has been made to ascertain the role of inter-electrode separation on the electrical, optical and structural properties of nc-Si:H films deposited by PE-CVD technique. The inter-electrode separation showed marked effect on these properties. The following aspects have been convincingly revealed by the above results. The deposition rate was observed maximum for the nc-Si:H film deposited at 30 mm inter-electrode separation. It decreases on both lower as well as higher inter-electrode separations. This result indicates that the deposition rate of nc-Si:H films critically depends up on the plasma chemistry/gas phase chemistry and hence inter-electrode separation. Raman spectroscopy and low angle X-ray diffraction spectra indicate that the films deposited at low inter-electrode separations (15 mm and 20 mm) are nanocrystalline whereas as nanocrystalline-to-amorphous transition has been for the films deposited at inter-electrode separation $>$ 20 mm. The FTIR spectroscopic analysis indicates that the nanocrystaline films have less bonded hydrogen content than the amorphous counterparts and can attributed to shifting of hydrogen bonding configuration from Si-H_2 and $(Si\text{-}H_2)_n$ bonded complexes to Si-H species with increase in inter-electrode separation. However, the band gap shows decreasing trend with increase in inter-electrode separation. The photosensitivity gain or photosensitivity enhances with inter-electrode separation can attributed to nanocrystalline-to-amorphous transition.

The authors SRJ, AMF, VSW and MMK are thankful Department of Science and Technology (DST) and Ministry of New and Renewable Energy (MNRE), Government of India and Centre for Nanomaterials and Quantum Systems (CNQS), University of Pune for the financial support.

REFERENCES

1. J. Yang, S. Guha, *Appl. Phys. Lett.* **61**, 2917 (1992).
2. S. Guha, J. Yang, A. Bannerjee, T. Glatfelter, K. Hoffman, S.R. Ovshinsky, M. Izu, H.C. Ovshinsky, X. Deng, *Mater. Res. Soc. Symp. Proc.* **336**, 645 (1994).
3. D.K. Staebler, C.R. Wronski, *Appl. Phys. Lett.* **31**, 292 (1977).
4. C. Lee, A. Sazonov, A. Nathan, *Appl. Phys. Lett.* **86**, 222106 (2005).
5. A.H. Mahan, *Sol. Energ Mat Sol. C* **78**, 299 (2003).
6. G. Bugnon, A. Feltrin, F. Meillaud J. Bailat, C. Ballif, *J. Appl. Phys.* **105**, 064507 (2009).

7. C. Niikura, M. Kondo, A. Matsuda, *J. Non-Cryst. Solids* **338-340**, 42 (2004).
8. E. Amanatides, D. Mataras, D.E. Rapakoulias, *J. Vac. Sci. Technol. A* **20**, 68 (2002).
9. A.V. Shah, J. Meier, E. Vallat-Sauvain, N. Wyrsch, U. Kroll, C. Droz, U. Graf, *Sol. Energ. Mat. Sol. C* **78**, 469 (2003).
10. C. Niikura, N. Itagaki, A. Matsuda, *Jpn. J. Appl. Phys.* **46**, 3052 (2007).
11. M. Isomura, M. Kondo, A. Matsuda, *Sol. Energ Mat Sol. C* **66**, 375 (2001.)
12. P. Kounavis, D. Mataras, N. Spiliopoulos, E. Mytilineou, D. Rapakoulias, *J. Appl. Phys.* **75**, 1599 (1994).
13. A. Matsuda, in *Springer Handbook of Electronic and Photonic Materials*, S. Kasap, P. Capper (Springer Science + Business Media: 2006).
14. M.J. Kushner, *J. Appl. Phys.* **63**, 2532 (1988).
15. E. Amanatides, D. Mataras, D.E. Rapakoulias, *J. Vac. Sci. Technol. A* **20**, 68 (2002).
16. D.W. Marquardt, *J. Soc. Ind. Appl. Math.* **11**, 431 (1963).
17. H. Miyahara, M. Takai, T. Nishimoto, M. Kondo, A. Matsuda, *Sol. Energ. Mat. Sol. C* **74**, 351 (2002).
18. A. Chowdhury, S. Mukhopadhyay, S. Ray, *Sol. Energ. Mat. Sol. C* **94**, 1522 (2010)
19. A. Singh, E.A. Devis, *J. Non-Cryst. Solids* **122**, 223 (1990).
20. J.C. Knights, G. Lucovsky, R.J. Nemanich, *J. Non-Crys. Solids* **32**, 393 (1979).
21. I. Montero, L. Galan, O. Najmi, J.M. Albella, *Phys. Rev. B* **50**, 4881 (1994).
22. D. Han, K. Wang, J. Owens, L. Nelson, H. Habachi, M. Tanaka, *J. Appl. Phys.* **93**, 3776 (2003).
23. P. John, I.M. Odeh, M.J.K. Thomas, *Solid State Commun.* **41**, 341 (1982).
24. H.R. Shanks, C.J. Fang, M. Cardona, F.J. Demond, S. Kalbitzer, *phys. status solidi B* **100**, 43 (1980).
25. M. Yamaguchi, K. Moigaki, *Phil. Mag. Part B* **79**, 387 (1999).
26. T. Saitoh, T. Shimada, M. Migitaka, Y. Tarui, *J. Non-Cryst. Solids* **59-60**, 715 (1983).